# GNSS-R Snow Depth Inversion Study Based on SNR-SVR

Yuan Hu, Jingxin Wang, Wei Liu, Xintai Yuan, and Jens Wickert

***Abstract*—The global navigation satellite system reflectometry (GNSS-R) technology has shown significant potential in retrieving snow depth using signal-to-noise ratio (SNR) data. However, compared to traditional in situ snow depth measurement techniques, we have observed that the accuracy and performance of GNSS-R can be significantly impacted under certain conditions, particularly when the elevation angle increases. This is due to the attenuation of the multipath effect, which is particularly evident during snow-free periods and under low-snow conditions where snow depths are below 50 cm. To address these limitations, we propose a snow depth inversion method that integrates SNR signals with the support vector regression algorithm, utilizing SNR sequences as feature inputs. We conducted studies at stations P351 and P030, covering elevation angles ranging from 5° to 20°, 5° to 25°, and 5° to 30°. The experimental results show that the root-mean-square error at both the stations decreased by 50% or more compared to traditional methods, demonstrating an improvement in inversion accuracy across different elevation angles. More importantly, the inversion accuracy of our method does not significantly lag behind that at lower elevation angles, indicating its excellent performance under challenging conditions. These findings highlight the contribution of our method in enhancing the accuracy of snow depth retrieval and its potential to drive further advancements in the field of GNSS-R snow depth inversion.**

***Index Terms*—Global navigation satellite system reflectometry (GNSS-R), signal-to-noise ratio (SNR), snow depth, support vector regression (SVR).**

## I. Introduction

THE study of snow depth is pivotal in numerous domains, including meteorological forecasting, climate research, ecological protection, disaster prevention, and fulfilling national economic and military needs. It serves as a crucial indicator not only for meteorological forecasting and climate analysis but also for maintaining ecological balance, mitigating natural disasters, and supporting economic and military operations. Through the observation and analysis of snow depth, we gain a deeper understanding of changes in the natural environment, providing a scientific foundation for informed decision making.

The global navigation satellite system (GNSS) has become a ubiquitous and essential infrastructure. This system encompasses several internationally recognized satellite navigation systems, such as the U.S. GPS, Russia's GLONASS, China's BDS, Europe's Galileo, Japan's QZSS, and India's NAVIC, along with various satellite-based augmentation systems. The GNSS has been extensively utilized in critical areas, such as navigation, timing, and positioning [1], and its applications are continuously expanding.

In recent decades, scientists have achieved remarkable advancements in the study of satellite signals, discovering that satellite reflection signals can be actively harnessed for the inversion of sea and land surface parameters. This application of reflection signals is known as the global navigation satellite system-reflectometry (GNSS-R) technique [2], [3], [4]. Martin-Neira [5] pioneered the potential use of GPS reflection signals for measuring sea surface parameters. Specifically, the signal-to-noise ratio (SNR) formed at the receiver antenna's phase center between direct and reflected satellite signals carries physical parameter information that is correlated with the depth of snow on the ground. Larson et al. [6] capitalized on this by utilizing the SNR data received by GPS receivers to invert snow depth. Their method exploited the frequency characteristics of the detrending term SNR data from the receiver to invert snow depth, resulting in inversions that aligned well with ultrasonic snow measurement instrument data near the stations. This milestone marked the beginning of GNSS-R snow depth inversion research. Furthermore, GNSS-R techniques have been extended to monitor sea ice thickness [7], [8], [9], land surface studies [10], [11], [12], [13], sea level height [14], [15], [16], [17], sea state [18], [19], [20], soil moisture [21], [22], [23], [24], and vegetation growth [25], [26], [27], demonstrating the versatility and potential of this technology.

Wang et al. [28] proposed a combined algorithm of fast Fourier transform (FFT) spectrum analysis and nonlinear least squares fitting (NLSF) for retrieving snow depth using GPS L1-band data. The NLSF algorithm demonstrated the highest accuracy when snow depth was below 80 cm, while the FFT algorithm performed best for snow depths above 80 cm. Their results showed a 10% improvement compared to the Lomb–Scargle Periodogram (LSP) spectrum analysis. Yu et al. [29] introduced a snow depth estimation method based on linear combinations of GPS triple-frequency signal multipath phases,

Received 26 June 2024; revised 22 August 2024; accepted 24 September 2024. Date of publication 2 October 2024; date of current version 11 October 2024. This work was supported in part by the National Natural Science Foundation of China under Grant 52071199. *(Corresponding author: Wei Liu.)*

Yuan Hu and Jingxin Wang are with The College of Engineering Science and Technology, Shanghai Ocean University, Shanghai 201306, China (e-mail: y-hu@shou.edu.cn; 3102903107@qq.com).

Wei Liu is with Merchant Marine College, Shanghai Maritime University, Shanghai 201306, China (e-mail: liu@sreil.com).

Xintai Yuan and Jens Wickert are with the Department of Geodesy, German Research Centre for Geosciences, 14473 Potsdam, Germany, and also with the Institute of Geodesy and Geoinformation Science, Berlin Institute of Technology, 10623 Berlin, Germany (e-mail: xt-yuan@foxmail.com; wickert@gfz-potsdam.de).

Digital Object Identifier 10.1109/JSTARS.2024.3470508

which showed improvement compared to traditional methods. Zhang et al. [30] proposed an improved snow depth retrieval method utilizing a combination of GNSS triple-frequency carrier phases. Compared with traditional triple-frequency snow depth retrieval methods, this method showed significant enhancement. Wan et al. [31] investigated the impact of terrain on GNSS interferometric reflectometry (GNSS-IR) and introduced the GSnow_TERR snow depth inversion model. This model considers terrain effects by incorporating the surface tilt angle ($\gamma$) into the derivative of the multipath relative phase ($\varphi$) concerning the satellite elevation angle ($\alpha$). The model's performance in practical applications was consistent with the theoretical analysis. Altuntas and Tunalioglu [32] presented a method to search for suitable satellite elevation angle ranges for each satellite orbit to improve snow depth retrieval. This method increased the snow depth correlation by 10.70% compared with traditional methods. Ma et al. [33] proposed a snow depth retrieval method based on multiazimuth and multisatellite data fusion for GNSS-IR, considering the impact of surface fluctuations. By compensating for errors in snow depth inversion values at different azimuths through the cluster analysis of reflector heights based on different satellites during nonsnow periods, they achieved a 5.04% increase in the correlation coefficient ($R$), a 43.49% reduction in the root-mean-square error (RMSE), and a 47.62% reduction in mean absolute error (MAE).

In recent years, the application of machine learning (ML) has garnered significant research interest, prompting numerous researchers to explore ML-based retrieval methods to enhance the efficiency and accuracy of traditional retrieval techniques. Zhan et al. [34] introduced a snow depth retrieval method utilizing a backpropagation neural network combined with the existing satellite data. This method achieved an RMSE of 0.0297 m and an MAE of 0.0219 m, demonstrating a high degree of consistency with measured data and a correlation coefficient of 0.9407. Altuntas et al. [35] proposed an ML classification method for snow depth retrieval using GNSS-IR technology. Through an ML classification algorithm, they classified strong and weak ground reconstructions using input parameters, such as azimuth angle, satellite elevation angle, year, reappearing signal amplitude, and epoch number. The results indicate that the classification performance of the ML classification algorithm is superior to traditional GNSS-IR algorithms. Liu et al. [36] presented a multifeature GNSS-R snow depth inversion method based on GA-BP neural networks. Compared to traditional methods, this approach achieved a 29.1% improvement in retrieval accuracy. Hu et al. [37] introduced a snow depth retrieval and snow detection algorithm for GNSS-R based on support vector machines (SVMs), which classifies and predicts snow-free and snow-covered states, achieving an overall detection accuracy of approximately 96%.

In traditional methods for retrieving snow depth, a common challenge is a significant decrease in retrieval accuracy as the satellite elevation angle increases. This phenomenon may be related to the weakening of the multipath effect on the signal as the elevation angle increases [38]. The current study further explores the potential factors affecting the accuracy of traditional methods and finds a close correlation between the low-frequency components extracted from LSP spectrum analysis and the decrease in retrieval accuracy of traditional methods. Specifically, these low-frequency components tend to result in overestimated snow depth values, particularly during nonsnow and snow periods with depths less than 50 cm. More crucially, as the elevation angle range increases, the number of signals detecting these low-frequency components also rises, exacerbating the decrease in retrieval accuracy. Consequently, as the elevation angle increases, the likelihood of LSP spectrum analysis identifying erroneous low-frequency components also rises, ultimately leading to significantly worse retrieval accuracy at high elevation angles compared with low angles. To address the issues encountered by traditional snow depth retrieval models, this study proposes a novel solution: utilizing SNR arc data as feature inputs for a support vector regression (SVR) inversion model. Experimental results show that by introducing ML techniques, we can better handle low-frequency signals and preserve their research potential. This method demonstrates excellent robustness and high retrieval accuracy across different elevation angle ranges, providing a new and effective solution in snow depth retrieval. The study not only addresses the problems of traditional snow depth retrieval models in processing low-frequency signals but also further explores the potential value of these signals, pointing to new directions for future research.

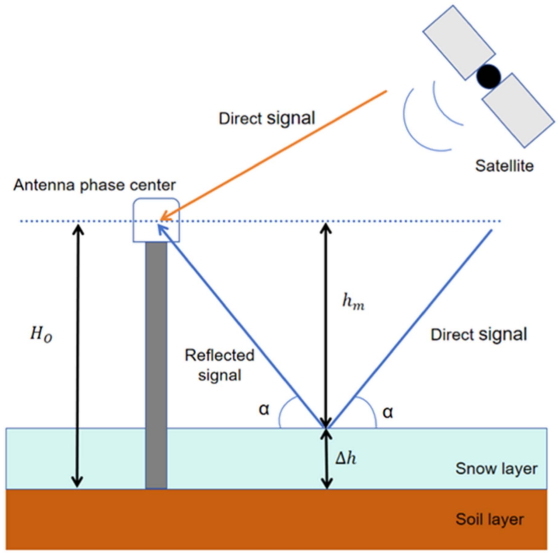


Fig. 1. Schematic of the GNSS-R inversion of snow depth.

The rest of this article is organized as follows. Section II primarily introduces the principles of GNSS-R snow depth retrieval, the SVR model, the SNR-SVR inversion method, and evaluation metrics. Section III describes the information, experimental results, and error analysis for the P351 and P030 stations separately. Finally, Section IV concludes this article.

## II. Methodology

### A. GNSS-R Snow Depth Inversion Principle

Fig. 1 presents a schematic diagram of the GNSS-R geometric model, illustrating the reception of both the direct signals from

a satellite and reflected signals from the ground at the antenna phase center. In this diagram, $H_o$ represents the distance from the antenna phase center to the ground, $h_m$ denotes the vertical distance from the antenna phase center to the ground reflection point, $\Delta h$ stands for the snow layer thickness, and $\alpha$ is the angle between the direct satellite signal and the ground. During the propagation of satellite signals, not only do the signals travel directly from the satellite to the receiving antenna, but they can also undergo refraction around the antenna, generating reflected signals that carry parameters related to the environmental information surrounding the antenna. By analyzing these reflected signals and their various parameters, including signal intensity, phase, frequency, and time delay, we can gain insights into the environmental conditions near the antenna. The superposition of the direct and reflected signals at the antenna phase center results in an interference signal, known as the SNR. This SNR signal can be expressed as the vector sum of the direct and reflected signals

$$\text{SNR} = A_d^2 + A_r^2 + 2A_dA_r\cos\phi \tag{1}$$

where $A_d$ represents the intensity of the direct signal, $A_r$ represents the intensity of the reflected signal, and $\phi$ denotes the delayed phase between the direct and reflected signals. The long-term trend of the SNR is primarily influenced by the direct signal, while the reflected signal contributes to the local fluctuations in the SNR. Commonly, a polynomial is fitted to the trend component of the SNR to isolate the direct signal portion. Subsequently, the detrended term (dSNR), which represents the reflected signal component, is obtained by subtracting the fitted trend from the original SNR. Specifically, at low satellite elevation angles, the dSNR can be modeled as a cosine function

$$\text{dSNR} = A\cos\left(2\pi f \sin\alpha + \phi\right) \tag{2}$$

where $A$ is the amplitude, $f$ is the oscillation frequency, and $\alpha$ is the satellite elevation angle. The frequency $f$ is obtained by the LSP analysis of the dSNR sequence. The following equation shows the relationship between the frequency $f$ and the reflector height $h_m$:

$$f = \frac{2h_m}{\lambda} \tag{3}$$

where $\lambda$ is the signal wavelength. Finally, the snow depth thickness $\Delta h$ is obtained by subtracting the antenna height $H_o$ from the reflector height $h_m$

$$\Delta h = H_0 - h_m. \tag{4}$$

### B. SVR Principle

SVR is a regression method that is grounded in the principles of SVM. Contrary to traditional linear regression, SVR transforms data into a high-dimensional space, employing the optimization algorithms of the SVM to establish a nonlinear regression model. The primary objective of SVR is to identify a function that minimizes the error between predicted and observed values while maximizing the margin within a specified tolerance. Specifically, SVR introduces a boundary, known as the support vector, to confine the error between predicted and observed values, while simultaneously optimizing the margin between the hyperplane (regression function) and these boundaries. Central to SVR is the utilization of kernel functions to transform data into a higher dimensional space, thereby capturing nonlinear relationships. Common kernel functions include the linear kernel, polynomial kernel, and radial basis function (RBF) kernel. These kernel functions can be selected based on the specific characteristics of the problem to enhance the model's fitting capabilities. Fig. 2 provides a schematic illustration of the principles underlying SVR.

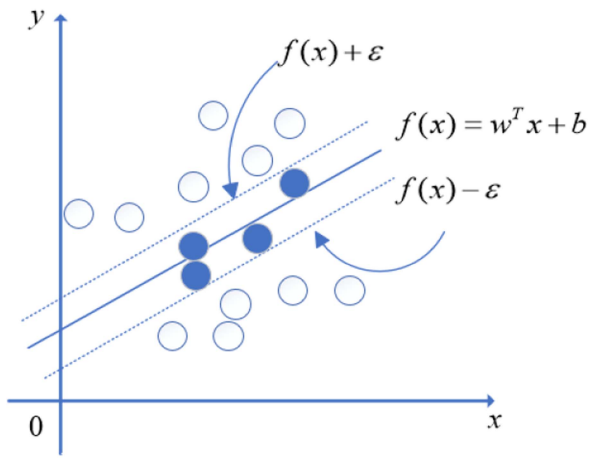


Fig. 2. Schematic diagram of SVR principle.

In the context of SVR, $w = (w_1, w_2, w_3, \ldots, w_n)$ represents the normal vector, which determines the direction of the hyperplane. $b$ is the displacement term, specifying the distance between the hyperplane and the origin. $x = (x_1, x_2, x_3, \ldots, x_n)$ denotes the sample set. $\varepsilon$ is the tolerance deviation, an empirical value set manually. For all the samples falling within the dashed lines, namely, the blue sample points, no loss is calculated. Only the loss for sample points outside the dashed lines is considered.

The core idea of SVR is to employ kernel functions to map data into a high-dimensional space, thereby enabling the capture of nonlinear relationships. Commonly used kernel functions include the linear kernel, polynomial kernel, and RBF kernel. These kernel functions can be selected based on the specific characteristics of the problem to achieve improved model-fitting performance.

Considering the specific characteristics of the data used in this study and the advantages of the RBF kernel function in handling complex nonlinear relationships, the RBF kernel function was selected as the kernel for the SVR model. For the RBF kernel, the $g$ parameter determines its width, which subsequently influences the model's sensitivity to data points and the degree of fitting. The penalty parameter $c$ controls the degree of tolerance to errors and the tradeoff between model complexity and the fit to the training data. The values of the hyperparameters vary for different sites, and the specific hyperparameter settings will be explained in subsequent experiments.

### C. SVR Snow Depth Inversion Method Based on SNR Arcs

As depicted in Fig. 3, the SNR signal exhibits notable oscillations at low elevation angles. As the elevation angle rises,

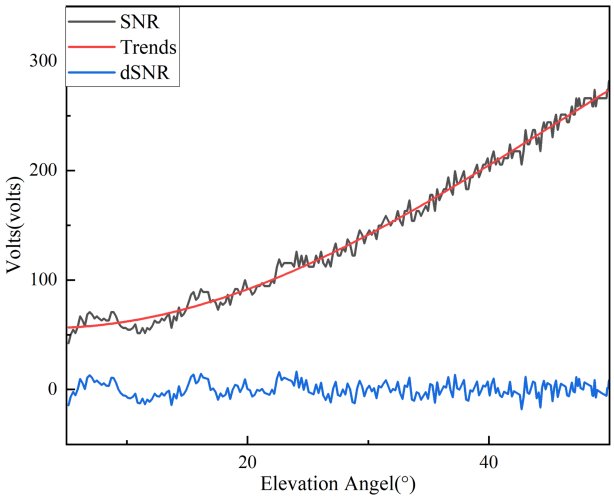


Fig. 3. G01 satellite observations on day 88 of 2021 at station P351: the black curve is the SNR signal, the red curve is the trend term fitted by a low-order polynomial, and the blue curve is the dSNR signal.

the oscillations diminish, and after the removal of the direct signal, the dSNR sequence gradually loses its cosine oscillation characteristics as the elevation angle increases. Consequently, it is common to study SNR signals at satellite elevation angles below 30°. During signal propagation, various environmental factors often introduce noise unrelated to surface snow information. These noises can manifest as overlapping peak interference and other abnormal phenomena during the LSP spectral analysis process [30], [39], which may lead to deviations in the analyzed frequency $f$ from its true value, thus resulting in inaccurate inversion of snow depth data.

Fig. 4 compares a disturbed spectral analysis result with an ideal healthy one. The figure reveals two distinct types of interference that can affect subsequent frequency extraction. First, Fig. 4(a) highlights a main peak in the spectrum, which is surrounded by noise. This noise obscures the clarity of the main peak, potentially causing errors in peak frequency extraction. Second, Fig. 4(c) depicts a secondary peak situated near the main peak. The presence of this secondary peak complicates the extraction of the main peak's frequency, as the algorithm may incorrectly identify it as the main peak or fail to accurately distinguish between the two.

To ensure the accuracy of snow depth retrieval data and eliminate anomalies, the data quality control (QC) process plays a pivotal role in this study. To achieve this, a series of QC indicators is utilized, encompassing satellite elevation angles as well as key LSP spectral analysis parameters, such as peak frequency, peak power, the ratio of peak to secondary peak power, and the ratio of peak to average power. These indicators are designed to identify and eliminate invalid data contaminated by interference. By employing this approach, we aim to improve the precision of snow depth retrieval and provide more reliable data to support related research and applications. The QC indicators are summarized in Table I.

After rigorous QC screening of the data, the traditional method for retrieving snow depth still produces anomalous

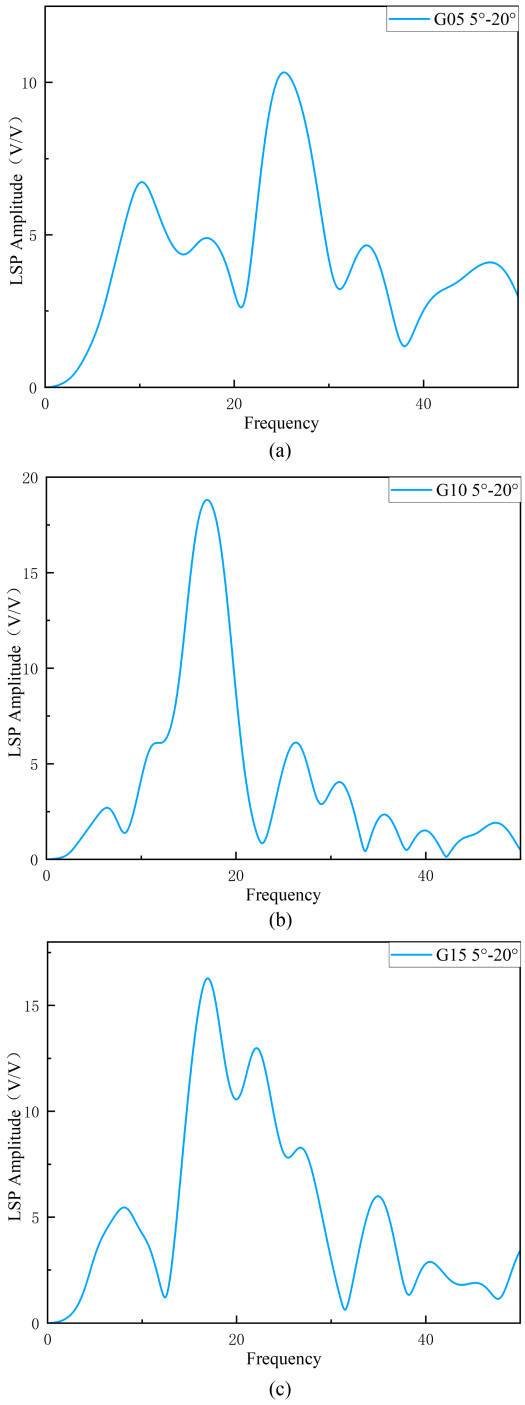


Fig. 4. LSP analysis plots. (a) Noise contaminated observations of G05 satellite on day 288 of 2021 at station P351. (b) Healthy observation results of G10 satellite on day 288 of 2021 at station P351. (c) Observations of G15 satellite contaminated by subpeak on day 8, 2016 at station P030.

values that exceed the reference snow depth on certain dates. Moreover, as the satellite elevation angle increases, the likelihood of these anomalous values occurring also rises. Through analysis, it has been determined that these anomalous values are attributed to abnormal LSP spectrum analysis results. Satellite signals that yield anomalous results exhibit low-frequency peaks during LSP spectrum analysis, resulting in the extraction of

TABLE I
QC INDICATORS

| Item | Processing strategies |
|---|---|
| Difference between maximum and minimum elevation angles | >10° |
| Peak powers | >2 V |
| Maximum peak power/average power | P351: >3.5 |
| | P030: >3 |
| Maximum peak power/sub-peak power | >1.9 |

low-frequency components. These low-frequency components correspond to computed snow depth data that are inconsistent with reality, significantly interfering with the accuracy of the traditional retrieval method.

To address the issue of anomalous values caused by abnormal spectrum analysis, this study proposes an SVR inversion model based on SNR raw arcs (SNR-SVR), which directly utilizes SNR arc data as input and leverages the effective information within the SNR arc data to estimate snow depth. The SNR-SVR method bypasses the intermediate steps of traditional methods, such as frequency extraction, thereby avoiding the extraction of anomalous frequencies due to external factors in traditional approaches. Experimental results show that using SNR arc data for snow depth inversion not only effectively avoids abnormal spectrum analysis but also achieves significantly higher inversion accuracy compared to traditional methods. Moreover, as the satellite elevation angle increases, this new method maintains excellent inversion accuracy and robustness.

The specific research process is outlined as follows: initially, we selected SNR signals with specific azimuth angles and satellite elevation angles. Subsequently, based on rigorously defined QC indicators, we conducted thorough QC on these SNR signals to ensure the selection of high-quality signals that meet the requirements. Then, using the maximum valid length of the filtered SNR signals as a benchmark, we performed linear interpolation on the remaining SNR signals to unify their dimensions. After unifying the dimensions, the SNR signals were subjected to normalization processing, followed by the adoption of a fivefold cross-validation approach to train an SVR model for predicting snow depth values. The predicted results were then comprehensively compared and evaluated against reference values. During the optimization of SVR model parameters, we employed the grid search method with the aim of minimizing the MAE as the criterion, ensuring the selection of optimal parameters that would enhance the predictive accuracy of the model. A flowchart of the experimental process is presented in Fig. 5.

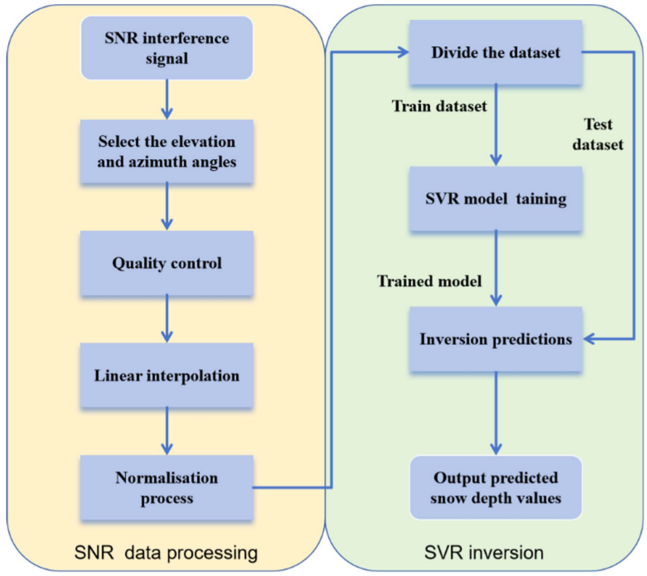


Fig. 5. Schematic of snow depth inversion.

### D. Evaluation Indicators

In this study, we employed three evaluation metrics: the coefficient of determination ($R^2$), the RMSE, and the MAE. $R^2$ measures the model's ability to explain the variability of the dependent variable, with a range from 0 to 1, where a value closer to 1 indicates a stronger explanatory power of the model for the observed values. The RMSE assesses the average magnitude of the error between the model's predictions and the actual observations, with a lower RMSE value indicating a better fit of the model to the actual observations. The MAE measures the average absolute error between the model's predictions and the actual observations, and a lower MAE value also signifies a better fit of the model to the actual observations. The specific expressions are as follows:

$$R^2 = 1 - \frac{\sum (Y_I - y_i)^2}{\sum (Y_I - \overline{Y})^2} \tag{5}$$

$$\mathrm{RMSE} = \sqrt{\frac{\sum (Y_I - y_i)^2}{n}} \tag{6}$$

$$\mathrm{MAE} = \frac{\sum |Y_I - y_i|}{n} \tag{7}$$

where $Y_I$ is the snow depth reference value for day $i$, $y_i$ is the predicted snow depth value for day $i$, $\overline{Y}$ is the mean value of the snow depth reference value, and $n$ is the total number of days.

## III. EXPERIMENTAL RESULTS AND ANALYSIS

### A. Station P351 and Data Sources

The P351 site (43.87441°N, 114.71916°W, and 2692.6 m), located in the city of Ketchum, United States, serves as an observation station within the EarthScope Plate Boundary Observatory (PBO) network. It is primarily used for measuring soil moisture, vegetation water content, and snow depth. The P351 site was commissioned on 30 August 2008, with an antenna height of approximately 2 m. Fig. 6(a) illustrates the site plan for site P351, revealing sparse vegetation, open ground, and relatively gentle topographic variations. The lack of obstructions facilitates sufficient signal reception by the antenna receiver, minimizing the influence of external factors, such as vegetation cover and topographic variations. The reference snow depth

(a)

(b)

Fig. 6. (a) Site map of station P351. (b) Schematic of the Galena Summit station.

values are obtained from the in situ snow depth measurements of the SNOTEL network's Galena Summit station (43.87497°N, 114.71363°W, and 2676 m), located approximately 500 m away from the P351 site, as shown in Fig. 6(b). In the SVR model used in this study, the $c$ parameter is 5, and the $g$ parameter is 0.5.

### B. Results of the Inversion Experiment at Station P351

For the GPS L1-band data collected by the station P351 over the entire year of 2021, this study specifically analyzed the data within the azimuth range of 0–360° and conducted analyses based on varying ranges of satellite elevation angles: 5–20°, 5–25°, and 5–30°. Subsequently, the inversion results derived from the SVR model were compared with those obtained from traditional algorithms. The specific outcomes of this comparison are presented in Table II.

Based on the results presented in Table II, it is evident that the accuracy of the traditional algorithm in retrieving snow depth significantly decreases with the increase in the elevation angle range, with a significant change in the RMSE up to 10 cm. Specifically, under the conditions of elevation angle ranges of 5–20°, 5–25°, and 5–30°, the traditional method achieved $R^2$ values of 94.43%, 88.32%, and 81.62%, respectively, with corresponding RMSE values of 12.44, 18.03, and 22.61 cm. The MAE values were 10.36, 13.64, and 16.26 cm. In contrast, the SNR-SVR inversion method demonstrated significant advantages. Even with the increase in the elevation angle range, the variation in its RMSE did not exceed 2 cm, not only achieving higher inversion accuracy than the traditional algorithm but also demonstrating excellent robustness.

The SNR-SVR achieved $R^2$ values of 98.98%, 98.45%, and 98.23% within different elevation angle ranges, representing improvements of 4.82%, 11.47%, and 20.34% compared to the traditional method, respectively. Meanwhile, its RMSE values were 5.33, 6.56, and 7.02 cm, representing improvements of 57.15%, 63.62%, and 68.55% over the traditional algorithm, respectively. In addition, the MAE values of SNR-SVR were 3.39, 4.29, and 4.68 cm, demonstrating improvement rates of 67.28%, 68.55%, and 71.22%, respectively. These results indicate that the SNR-SVR method exhibits higher accuracy and stronger stability in snow depth inversion.

As depicted in Fig. 7, the performance of the SNR-SVR model and the traditional algorithm in snow depth inversion under different satellite elevation angle ranges is compared. The horizontal axis represents time, while the vertical axis corresponds to the snow depth values. It can be observed from Fig. 7 that the overall trends of the traditional algorithm (blue curve) and the SNR-SVR inversion method (red curve) are generally consistent with the reference snow depth values (black curve), but the inversion results of the SNR-SVR model outperform the traditional algorithm overall.

Fig. 8 presents the error plots of the two inversion methods under different elevation angle ranges. By carefully examining the results and error plots of the two methods, it can be noticed that the traditional algorithm exhibits a tendency of discrete snow depth values over some dates as the elevation angle range increases. Specifically, as the elevation angle range expands, the errors of the traditional algorithm gradually increase, and the number of dates with larger errors also gradually increases. In contrast, the SNR-SVR inversion method does not show a similar trend of varying with the elevation angle. Regardless of whether the elevation angle range is 5–20° or 5–30°, the inversion results of the SNR-SVR remain consistent with small fluctuations. The inversion errors under different elevation angle ranges are all controlled within a small range, which fully demonstrates the high accuracy and stability of the SNR-SVR inversion method.

These results indicate that the SNR-SVR model exhibits significant advantages in snow depth inversion, especially under conditions of high elevation angles, where it maintains stable inversion accuracy.

### C. Station P030 and Data Sources

The station P030 (41.7498°N, 110.5128°W, and 2149.8 m) is located in the city of Kemmerer, United States, and serves as an observation site within the EarthScope PBO network. It is used for measuring soil moisture, vegetation water content, and snow

TABLE II
STATISTICS OF THE RESULTS OF THE TRADITIONAL METHOD (TR) AND THE SNR-SVR INVERSION METHOD FOR STATION P351 AT DIFFERENT ELEVATION RANGES IN 2021

| Elevation angle | Methods | Precision indicators | | | Enhancement ratio | | |
|---|---|---|---|---|---|---|---|
| | | $R^2$ (%) | RMSE (cm) | MAE (cm) | $R^2$ (%) | RMSE (%) | MAE (%) |
| 5–20° | TR | 94.43 | 12.44 | 10.36 | **4.82** | **57.15** | **67.28** |
| | **SNR-SVR** | **98.98** | **5.33** | **3.39** | | | |
| 5–25° | TR | 88.32 | 18.03 | 13.64 | **11.47** | **63.62** | **68.55** |
| | **SNR-SVR** | **98.45** | **6.56** | **4.29** | | | |
| 5–30° | TR | 81.62 | 22.61 | 16.26 | **20.34** | **68.95** | **71.22** |
| | **SNR-SVR** | **98.23** | **7.02** | **4.68** | | | |

The bold values emphasize the results of the SNR-SVR model, aiming to provide an intuitive and striking comparison with traditional methods.

TABLE III
STATISTICS OF THE RESULTS OF THE TR AND SNR-SVR INVERSION METHOD FOR STATION P030 AT DIFFERENT ELEVATION RANGES IN 2016

| Elevation angle | Methods | Precision indicators | | | Enhancement ratio | | |
|---|---|---|---|---|---|---|---|
| | | $R^2$ (%) | RMSE (cm) | MAE (cm) | $R^2$ (%) | RMSE (%) | MAE (%) |
| 5–20° | TR | 93.54 | 3.72 | 3.24 | **4.67** | **43.01** | **55.25** |
| | **SNR-SVR** | **97.91** | **2.12** | **1.45** | | | |
| 5–25° | TR | 84.39 | 5.78 | 4.15 | **13.86** | **50** | **54.7** |
| | **SNR-SVR** | **96.09** | **2.89** | **1.88** | | | |
| 5–30° | TR | 73.92 | 7.48 | 4.79 | **24.95** | **51.34** | **50.94** |
| | **SNR-SVR** | **93.84** | **3.64** | **2.35** | | | |

The bold values emphasize the results of the SNR-SVR model, aiming to provide an intuitive and striking comparison with traditional methods.

depth. The station P030 was put into operation on 8 September 2005, surrounded by an open and gently sloping terrain, making it suitable for snow depth research, as shown in Fig. 9. The reference antenna height value is based on the average reflector height during the nonsnow period obtained by Larson and Small [40] at the station P030, which is approximately 1.8 m. Due to the relatively large distance between the station P030 and the nearby SNOTEL snow depth measurement stations, the snow depth reference values are obtained from the PBO H2O website. In the SVR model used in this study, the $c$ parameter is 6, and the $g$ parameter is 0.229.

### *D. Results of the Inversion Experiment at Station P030*

Similar to the station P351, the station P030 utilized GPS L1-band data from days 1 to 182 of 2016, selecting data within the azimuth range of 0–360°, and conducting analyses based on different satellite elevation angle ranges (5–20°, 5–25°, and 5–30°). The inversion results obtained from the SNR-SVR model were compared with those of traditional algorithms, as detailed in Table III.

As can be seen from Table III, the traditional method exhibited the highest inversion accuracy when the elevation angle ranged from 5–20°. However, as the elevation angle range increased, the inversion accuracy gradually decreased. Specifically, under the conditions of elevation angles ranging from 5–20°, 5–25°, and 5–30°, the $R^2$ values of the traditional method were 93.54%, 84.39%, and 73.92%, respectively, with corresponding RMSEs of 3.72, 5.78, and 7.48 cm, and MAEs of 3.24, 4.15, and 4.79 cm. In contrast, the SNR-SVR inversion method performed significantly better. It not only surpassed the traditional method in terms of accuracy but also showed a significantly lower variation in inversion accuracy across different elevation angle ranges of SNR data, demonstrating its excellent robustness. Under the conditions of elevation angles ranging from 5–20°, 5–25°, and 5–30°, the $R^2$ values of the SNR-SVR inversion method were 97.91%, 96.09%, and 93.84%, respectively, representing improvements of 4.67%, 13.86%, and 24.95% compared to the traditional method. In addition, the RMSEs were 2.12, 2.89, and 3.64 cm, representing improvements of 43.01%, 50%, and 51.34% compared to the traditional method. Furthermore, the MAEs of the SNR-SVR method were 1.45, 1.88, and 2.35 cm, representing improvements of 55.25%, 54.7%, and 50.94% compared to the traditional method, respectively. These results fully demonstrate that the SNR-SVR inversion method exhibits higher accuracy and stronger stability in handling SNR data with different elevation angle ranges.

The comparison of the two snow depth inversion results, as shown in Fig. 10, reveals significant differences in the performance of the SNR-SVR model and the traditional algorithm under different satellite elevation angle ranges. The horizontal axis represents time, while the vertical axis indicates the snow depth values. By comparing the trends of the traditional algorithm (blue curve) and the SNR-SVR inversion method (red curve) with the reference snow depth values (black curve), it is evident that although both the methods follow the general trend of the true values, the overall performance of the SNR-SVR model inversion results is significantly better than the traditional algorithm.

Fig. 11 illustrates the inversion errors of the two methods across different elevation angle ranges. A detailed analysis of

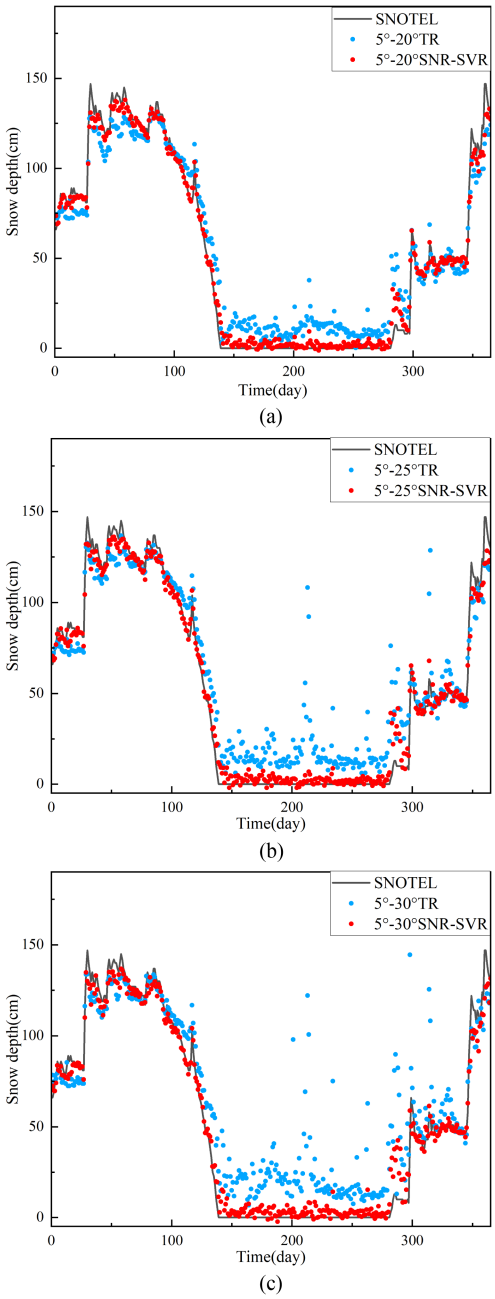


Fig. 7. Schematic representation of the results of the traditional and SNR-SVR inversion methods for station P351 in 2021 for different elevation angle ranges. (a) Elevation angle 5–20°. (b) Elevation angle 5–25°. (c) Elevation angle 5–30°.

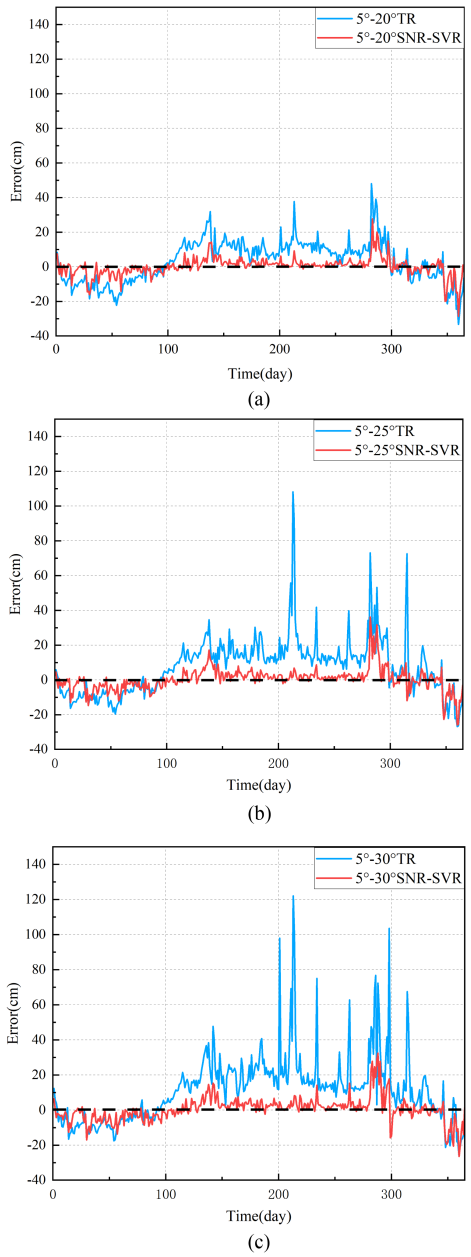


Fig. 8. Schematic representation of the error results of the conventional and SNR-SVR inversion methods for station P351 in 2021 for different elevation angle ranges. (a) Elevation angle 5–20°. (b) Elevation angle 5–25°. (c) Elevation angle 5–30°.

the inversion results and error plots reveals that the traditional algorithm exhibits outliers in its inversion results, and these outliers become more prominent as the elevation angle range increases. Whether during the snowy period or nonsnowy period, some outliers significantly deviate from the real-world situation, with the maximum error even reaching 50 cm. This undoubtedly compromises the stability of the overall inversion accuracy.

In contrast, the SNR-SVR inversion method exhibits clear advantages. Regardless of the change in the elevation angle range, its inversion results consistently closely align with the reference snow depth values, without exhibiting outliers or significant error increases, as seen in the traditional algorithm, especially at higher elevation angles. The overall error of the SNR-SVR inversion method is controllable, and the error trends across different elevation angle ranges tend to be consistent. This indicates that its inversion results are more stable and accurate than the traditional algorithm.

### *E. Analysis of Snow Depth Inversion Errors*

Figs. 12 and 13 display the LSP spectral analysis results and their corresponding reflector heights for some anomalous SNR signals recorded at stations P351 and P030, respectively.

TABLE IV
COMPARISON OF THE RESULTS OF SOME ANOMALOUS SNR SIGNALS CORRESPONDING TO TRADITIONAL AND SNR-SVR INVERSION METHODS

| Site | Day of year | Elevation angle | Satellite number | TR (cm) | SNR-SVR (cm) | Snow depth reference (cm) |
|---|---|---|---|---|---|---|
| P351 | 286 | 5–20° | G07 | 71.56 | **15.27** | 13 |
| | 213 | 5–25° | G01 | 133.03 | **1.93** | 0 |
| | 134 | 5–30° | G22 | 141.04 | **28.05** | 25 |
| P030 | 117 | 5–20° | G31 | 110.93 | **13.19** | 0 |
| | 2 | 5–25° | G19 | 86.1 | **20.87** | 21 |
| | 77 | 5–30° | G24 | 133.65 | **8.63** | 7 |

The bold values emphasize the results of the SNR-SVR model, aiming to provide an intuitive and striking comparison with traditional methods.

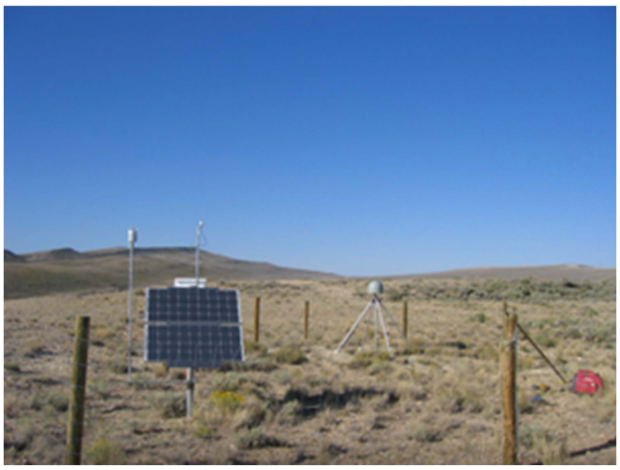

Fig. 9. Schematic of the P030 site.

In these two figures, the blue dashed lines correspond to the reflector heights ($h$) associated with the peak frequencies ($f$) extracted from the LSP spectral analysis, while the red dashed lines represent the true frequencies ($F$) and their corresponding reflector heights ($H$). After observing the snow depth inversion results at these two stations, we noticed the occurrence of anomalous values when using the traditional method for snow depth inversion. Further analysis revealed that as the elevation angle range increases, the frequency of occurrence of anomalous snow depth values also rises. These anomalous values originate from the low frequencies extracted by the LSP spectral analysis, leading to lower calculated reflector heights and subsequently creating a false impression of higher snow depths that do not align with reality. Although the LSP spectral analysis results of these anomalous SNR signals may appear normal at first glance, their discrepancy with the actual conditions ultimately has a significant negative impact on the overall accuracy of snow depth inversion.

Table IV compares the results of two different inversion methods for some anomalous signals, including the traditional method and the SNR-SVR inversion method. From the data presented in Table IV, it can be observed that the traditional method exhibits significant deviations between the inverted results and the reference snow depth values when faced with anomalous signals. Notably, during the no-snow period, the traditional method erroneously inverted snow depth data up to over 100 cm, undoubtedly posing significant challenges to snow depth inversion. In contrast, the SNR-SVR inversion method effectively avoids the interference of low-frequency components by bypassing the spectral analysis process. Its inversion results not only have higher accuracy but also have errors that are controlled within a small range when compared to the reference snow depth values, having a very limited impact on the final inversion accuracy. This result once again demonstrates the high precision and robustness of the SNR-SVR inversion method, enabling it to provide more accurate and reliable snow depth inversion results when faced with anomalous signals.

### F. Discussion

The experimental results presented earlier indicate a gradual increase in errors when utilizing traditional methods for snow depth retrieval as satellite elevation angles increase. Notably, this error phenomenon is particularly pronounced during nonsnow periods and low-snow depths below 50 cm. Through intensive research, we have discovered a close correlation between the low-frequency components extracted from LSP spectral analysis and the decline in retrieval accuracy using traditional methods. This phenomenon may be attributed to the attenuation of the multipath effect as satellite elevation angles increase. In contrast, the SNR-SVR snow depth retrieval model exhibits significantly superior retrieval accuracy across various satellite elevation angles, demonstrating robust performance. Furthermore, it is evident that even satellite signals with abnormal frequencies retain crucial research value.

Due to its formulaic nature, the traditional method can quickly process datasets and has advantages in computational efficiency compared with the SNR-SVR model. Specifically, at Station P351, when processing 10 449 samples, the traditional method consumed 16.67 s, whereas the SNR-SVR model initially took 54.23 s. However, upon implementing parallel computing [41], the computation time of the SNR-SVR model was significantly reduced to 10.85 s. Similarly, at Station P030 with 5928 samples, the traditional method required 9.81 s, while the standalone SNR-SVR model needed 22.85 s. Nevertheless, the incorporation of parallel computing drastically decreased the SNR-SVR model's computation time to 4.57 s. Notably, the SNR-SVR model surpasses traditional methods in terms of prediction accuracy and robustness, particularly demonstrating smaller errors at high satellite elevations. Consequently, although the

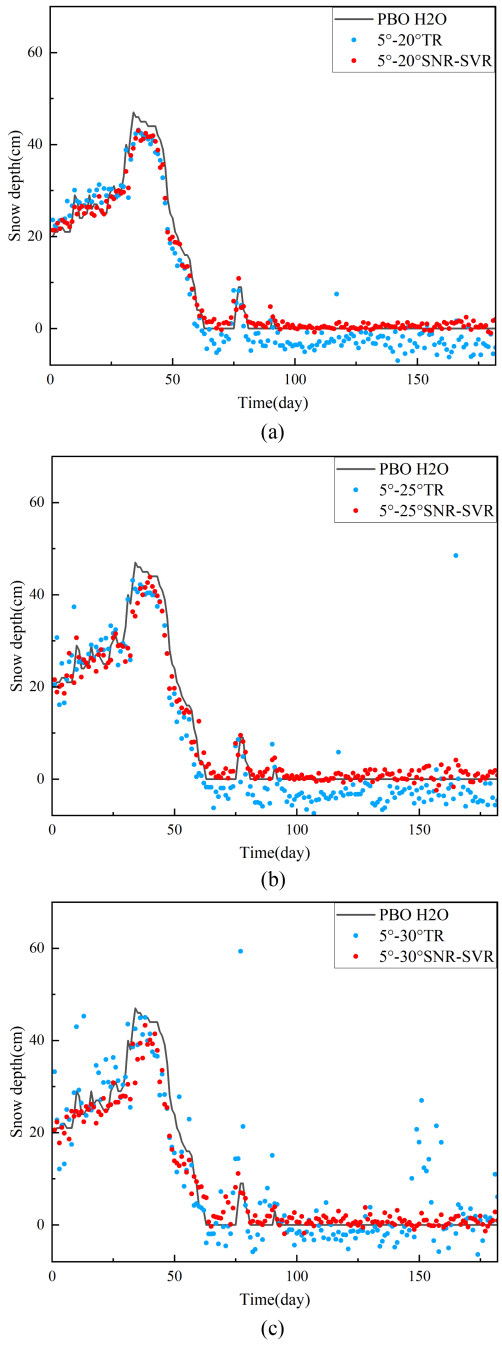


Fig. 10. Schematic representation of the results of the traditional and SNR-SVR inversion methods for station P030 in 2016 at different elevation angle ranges. (a) Elevation angle 5–20°. (b) Elevation angle 5–25°. (c) Elevation angle 5–30°.

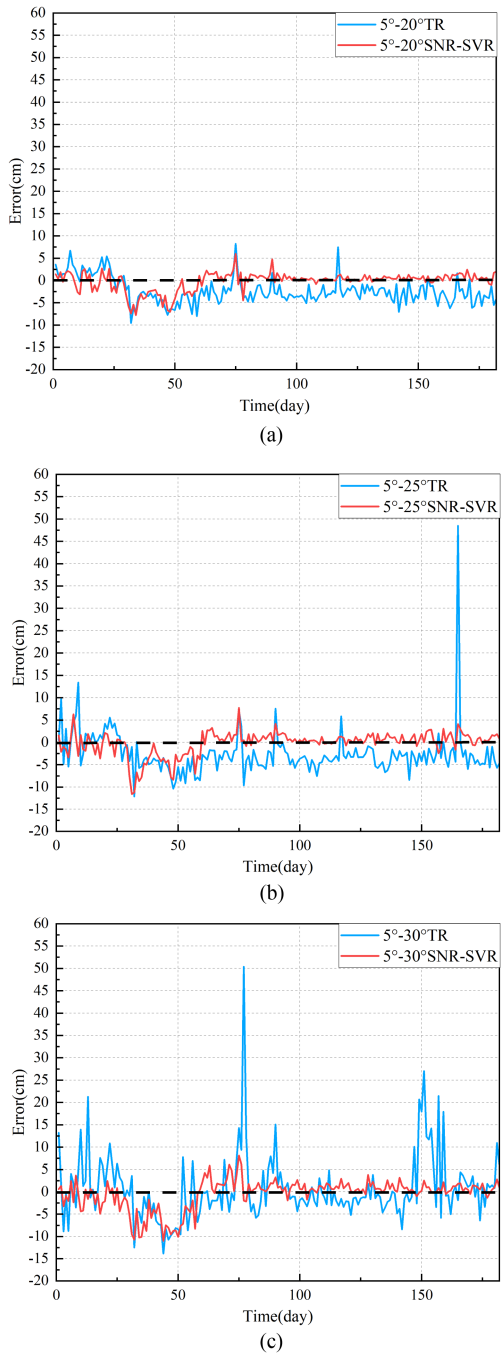


Fig. 11. Schematic representation of the error results of the traditional and SNR-SVR inversion methods for station P030 in 2016 at different elevation angle ranges. (a) Elevation angle 5–20°. (b) Elevation angle 5–25°. (c) Elevation angle 5–30°.

SNR-SVR model may exhibit slightly lower efficiency when operating independently, its combination with parallel computing for data processing provides distinct advantages in handling such scenarios.

In our investigation of snowfall observation data from stations P351 and P030, we uncovered a notable phenomenon: when snow depths at station P351 exceeded 50 cm, the observed data exhibited a pronounced negative bias. Similarly, station P030 predominantly demonstrated a tendency for predicted snow depths to be smaller than the actual values, particularly during the critical period of rapid snow accumulation and ablation, spanning days 30 to 59. This phenomenon is hypothesized to stem from the penetration effect of direct signals through the snowpack. Specifically, the delay path of the signals increases significantly upon traversing the snow layer, a physical process that leads to an anomalous elevation of the reflector height, subsequently resulting in a systematic underestimation of snow depth estimates [42]. Furthermore, it is noteworthy that during

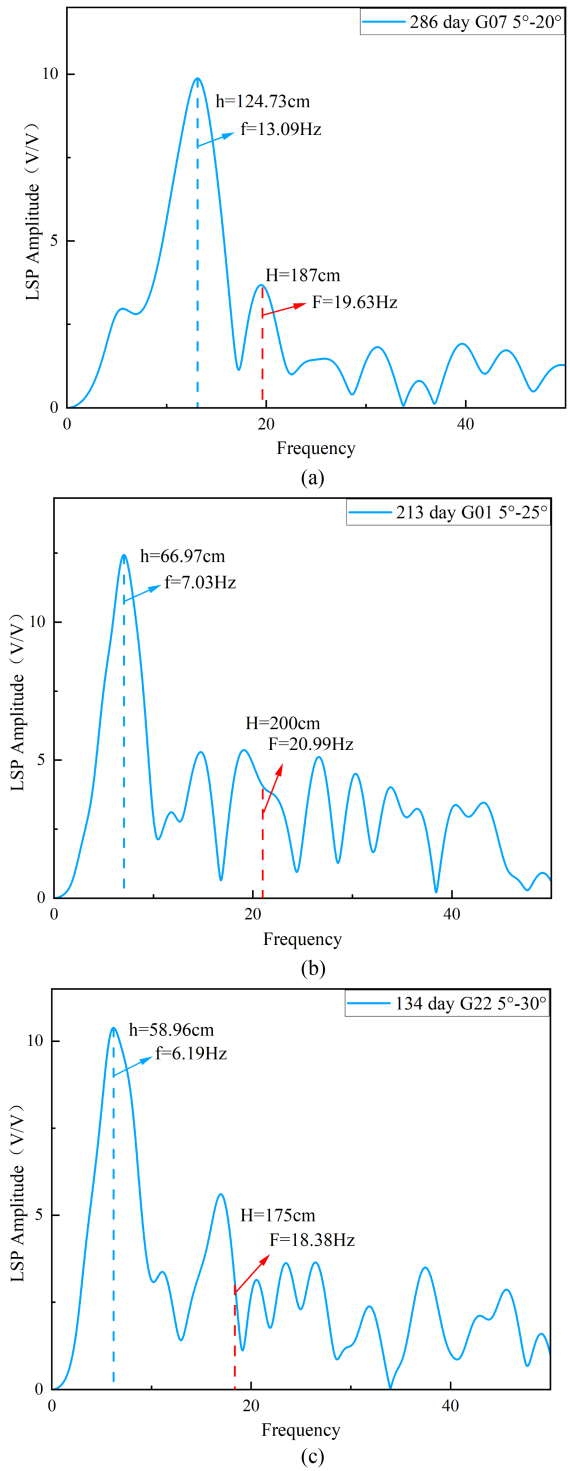


Fig. 12. Results of the LSP spectral analysis of some anomalous SNR signals at station P351. (a) Day 286 G07 satellite. (b) Day 213 G01 satellite. (c) Day 134 G22 satellite.

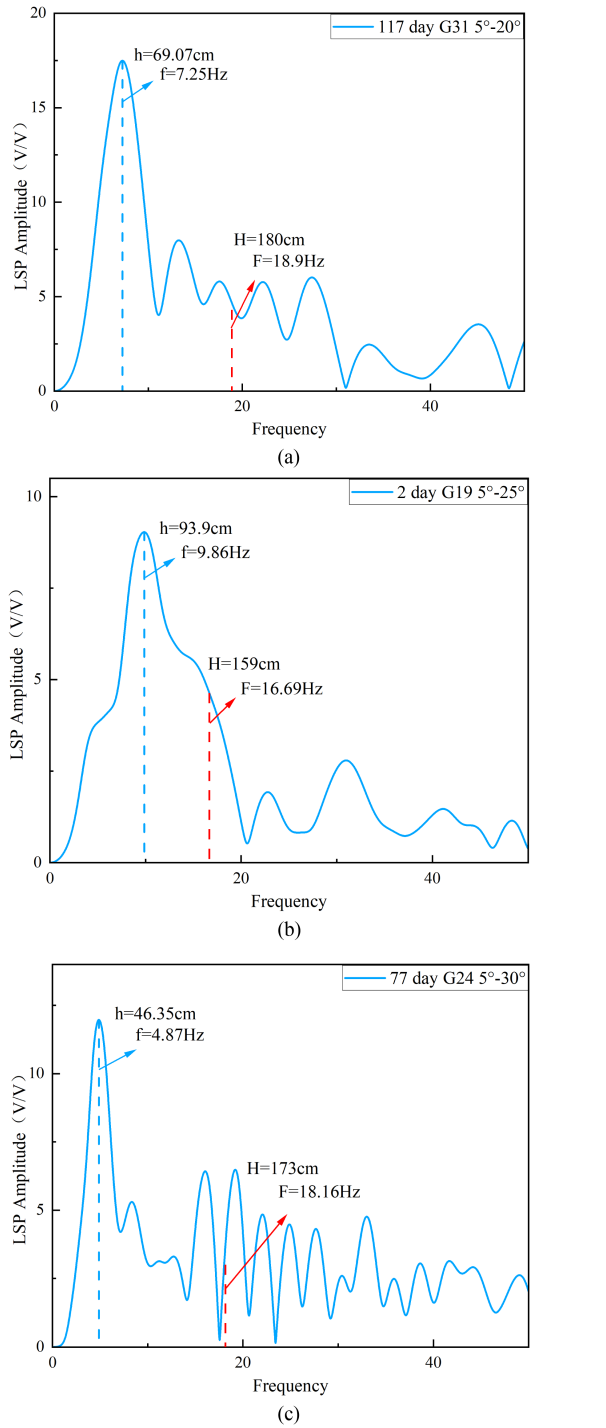


Fig. 13. Results of the LSP spectral analysis of some anomalous SNR signals at station P030. (a) Day 117 G31 satellite. (b) Day 2 G19 satellite. (c) Day 77 G24 satellite.

the final stages of snowmelt, specifically days 130 to 139 at station P351 and days 59 to 63 at station P030, the predicted snow depths unexpectedly surpassed the true values. We speculate that this anomaly is intimately linked to the rapid changes in surface snow conditions, where SNR data collected within the same day may contain a complex mixture of information from both the snow-covered and snow-free (or thinly snow-covered) areas [37]. This blend of information significantly complicates the accurate interpretation of snow depth, posing additional challenges to snow depth research. Consequently, future studies must meticulously consider these dynamic factors to enhance the precision and reliability of snow depth estimations.

## IV. Conclusion

As the satellite elevation angle increases, the multipath effect weakens, resulting in a decrease in the inversion accuracy of traditional methods. Specifically, the LSP spectral analysis extracts low-frequency components during the snow-free period and when the snow depth is below 50 cm, leading to inaccurately high snow depth values that drag down the inversion accuracy. To address this issue, we propose a snow depth inversion method that combines SNR signals with the SVR algorithm, utilizing the SNR sequence as the feature input. This method does not rely on antenna height data and directly skips the cumbersome signal spectral analysis step in traditional methods, thus avoiding the adverse impact of potentially unstable spectral analysis results on inversion accuracy.

In analyzing the causes of the low-frequency components in anomalous satellite signals, we have noticed that these signals still have research potential. When dealing with satellite data from different elevation angle ranges, our constructed SNR-SVR inversion model exhibits excellent robustness, outperforming traditional methods. Under the same experimental conditions, the SNR-SVR model demonstrates higher precision in snow depth inversion. Looking ahead, this method not only simplifies the retrieval process, enhances retrieval accuracy, and improves robustness, but also holds significant potential for further application in environmental fields, such as ocean remote sensing, soil moisture and land surface studies, as well as ice monitoring, showcasing its broad potential and applied value.

## References


[1] J. M. Dow, R. E. Neilan, and C. Rizos, "The international GNSS service in a changing landscape of global navigation satellite systems," *J. Geodesy*, vol. 83, no. 3, pp. 191–198, Mar. 2009, doi: 10.1007/s00190-008-0300-3.

[2] A. Bilich, K. M. Larson, and P. Axelrad, "Observations of signal-to-noise ratios (SNR) at geodetic GPS site CASA: Implications for phase multipath," *Proc. Century Eur. Geodyn. Seismol.*, vol. 23, pp. 77–83, 2004.

[3] R. Shah and J. L. Garrison, "Application of the ICF coherence time method for ocean remote sensing using digital communication satellite signals," *IEEE J. Sel. Top. Appl. Earth Observ. Remote Sens.*, vol. 7, no. 5, pp. 1584–1591, May 2014, doi: 10.1109/JSTARS.2014.2314531.

[4] Q. Yan, W. Huang, and C. Moloney, "Neural networks based sea ice detection and concentration retrieval from GNSS-R delay-Doppler maps," *IEEE J. Sel. Top. Appl. Earth Observ. Remote Sens.*, vol. 10, no. 8, pp. 3789–3798, Aug. 2017, doi: 10.1109/JSTARS.2017.2689009.

[5] M. Martin-Neira, "A passive reflectometry and interferometry system (PARIS): Application to ocean altimetry[J]," *ESA J.*, vol. 17, no. 4, pp. 331–355, 1993.

[6] K. M. Larson, E. D. Gutmann, V. U. Zavorotny, J. J. Braun, M. W. Williams, and F. G. Nievinski, "Can we measure snow depth with GPS receivers?," *Geophys. Res. Lett.*, vol. 36, no. 17, Sep. 2009, doi: 10.1029/2009GL039430.

[7] J. Strandberg, T. Hobiger, and R. Haas, "Coastal sea ice detection using ground-based GNSS-R," *IEEE Geosci. Remote Sens. Lett.*, vol. 14, no. 9, pp. 1552–1556, Sep. 2017, doi: 10.1109/LGRS.2017.2722041.

[8] Y. Xie and Q. Yan, "Stand-alone retrieval of sea ice thickness from FY-3E GNOS-R data," *IEEE Geosci. Remote Sens. Lett.*, vol. 21, 2024, Art. no. 2000305, doi: 10.1109/LGRS.2024.3352831.

[9] A. Regmi, M. E. Leinonen, A. Pärssinen, and M. Berg, "Monitoring sea ice thickness using GNSS-interferometric reflectometry," *IEEE Geosci. Remote Sens. Lett.*, vol. 19, 2022, Art. no. 2001405, doi: 10.1109/LGRS.2022.3198189.

[10] Q. Yan, S. Liu, T. Chen, S. Jin, T. Xie, and W. Huang, "Mapping surface water fraction over the pan-tropical region using CYGNSS data," *IEEE Trans. Geosci. Remote Sens.*, vol. 62, 2024, Art. no. 5800914, doi: 10.1109/TGRS.2024.3394744.

[11] Y. Jia, P. Savi, D. Canone, and R. Notarpietro, "Estimation of surface characteristics using GNSS LH-reflected signals: Land versus water," *IEEE J. Sel. Top. Appl. Earth Observ. Remote Sens.*, vol. 9, no. 10, pp. 4752–4758, Oct. 2016, doi: 10.1109/JSTARS.2016.2584092.

[12] T. Yang et al., "Land surface characterization using BeiDou signal-to-noise ratio observations," *GPS Solutions*, vol. 23, no. 2, Jan. 2019, Art. no. 32, doi: 10.1007/s10291-019-0824-4.

[13] Y. Chen and Q. Yan, "Unlocking the potential of CYGNSS for pan-tropical inland water mapping through multi-source data and transformer," *Int. J. Appl. Earth Observ. Geoinf.*, vol. 133, Sep. 2024, Art. no. 104122, doi: 10.1016/j.jag.2024.104122.

[14] K. M. Larson, J. S. Löfgren, and R. Haas, "Coastal sea level measurements using a single geodetic GPS receiver," *Adv. Space Res.*, vol. 51, no. 8, pp. 1301–1310, 2013.

[15] J. S. Löfgren and R. Haas, "Sea level measurements using multi-frequency GPS and GLONASS observations," *EURASIP J. Adv. Signal Process.*, vol. 2014, no. 1, Dec. 2014, Art. no. 50, doi: 10.1186/1687-6180-2014-50.

[16] J. Strandberg, T. Hobiger, and R. Haas, "Improving GNSS-R sea level determination through inverse modeling of SNR data," *Radio Sci.*, vol. 51, no. 8, pp. 1286–1296, Aug. 2016, doi: 10.1002/2016RS006057.

[17] X. Wang, X. He, and Q. Zhang, "Evaluation and combination of quad-constellation multi-GNSS multipath reflectometry applied to sea level retrieval," *Remote Sens. Environ.*, vol. 231, Sep. 2019, Art. no. 111229, doi: 10.1016/j.rse.2019.111229.

[18] F. Soulat, M. Caparrini, O. Germain, P. Lopez-Dekker, M. Taani, and G. Ruffini, "Sea state monitoring using coastal GNSS-R," *Geophys. Res. Lett.*, vol. 31, no. 21, 2004, Art. no. L21303, doi: 10.1029/2004GL020680.

[19] N. Roussel et al., "Sea level monitoring and sea state estimate using a single geodetic receiver," *Remote Sens. Environ.*, vol. 171, pp. 261–277, Dec. 2015, doi: 10.1016/j.rse.2015.10.011.

[20] M. Hoseini et al., "On the response of polarimetric GNSS-reflectometry to sea surface roughness," *IEEE Trans. Geosci. Remote Sens.*, vol. 59, no. 9, pp. 7945–7956, Sep. 2021, doi: 10.1109/TGRS.2020.3031396.

[21] K. M. Larson, E. E. Small, E. Gutmann, A. Bilich, P. Axelrad, and J. Braun, "Using GPS multipath to measure soil moisture fluctuations: Initial results," *GPS Solutions*, vol. 12, no. 3, pp. 173–177, Jul. 2008, doi: 10.1007/s10291-007-0076-6.

[22] N. Rodriguez-Alvarez et al., "Soil moisture retrieval using GNSS-R techniques: Experimental results over a bare Soil field," *IEEE Trans. Geosci. Remote Sens.*, vol. 47, no. 11, pp. 3616–3624, Nov. 2009, doi: 10.1109/TGRS.2009.2030672.

[23] N. Roussel et al., "Detection of soil moisture variations using GPS and GLONASS SNR data for elevation angles ranging from 2° to 70°," *IEEE J. Sel. Top. Appl. Earth Observ. Remote Sens.*, vol. 9, no. 10, pp. 4781–4794, Oct. 2016, doi: 10.1109/JSTARS.2016.2537847.

[24] Q. Yan, W. Huang, S. Jin, and Y. Jia, "Pan-tropical soil moisture mapping based on a three-layer model from CYGNSS GNSS-R data," *Remote Sens. Environ.*, vol. 247, Sep. 2020, Art. no. 111944, doi: 10.1016/j.rse.2020.111944.

[25] N. Rodriguez-Alvarez et al., "Land geophysical parameters retrieval using the interference pattern GNSS-R technique," *IEEE Trans. Geosci. Remote Sens.*, vol. 49, no. 1, pp. 71–84, Jan. 2011, doi: 10.1109/TGRS.2010.2049023.

[26] N. Rodriguez-Alvarez et al., "Review of crop growth and soil moisture monitoring from a ground-based instrument implementing the interference pattern GNSS-R technique," *Radio Sci*, vol. 46, no. 06, pp. 1–11, Dec. 2011, doi: 10.1029/2011RS004680.

[27] A. Egido et al., "Global navigation satellite systems reflectometry as a remote sensing tool for agriculture," *Remote Sens.*, vol. 4, no. 8, pp. 2356–2372, Aug. 2012, doi: 10.3390/rs4082356.

[28] X. Wang, S. Zhang, L. Wang, X. He, and Q. Zhang, "Analysis and combination of multi-GNSS snow depth retrievals in multipath reflectometry," *GPS Solutions*, vol. 24, no. 3, May 2020, Art. no. 77, doi: 10.1007/s10291-020-00990-3.

[29] K. Yu, W. Ban, X. Zhang, and X. Yu, "Snow depth estimation based on multipath phase combination of GPS triple-frequency signals," *IEEE Trans. Geosci. Remote Sens.*, vol. 53, no. 9, pp. 5100–5109, Sep. 2015, doi: 10.1109/TGRS.2015.2417214.

[30] Z. Zhang, F. Guo, and X. Zhang, "Triple-frequency multi-GNSS reflectometry snow depth retrieval by using clustering and normalization algorithm to compensate terrain variation," *GPS Solutions*, vol. 24, no. 2, Mar. 2020, Art. no. 52, doi: 10.1007/s10291-020-0966-4.

[31] W. Wan et al., "Toward terrain effects on GNSS interferometric reflectometry snow depth retrievals: Geometries, modeling, and applications," *IEEE Trans. Geosci. Remote Sens.*, vol. 60, 2022, Art. no. 4415514, doi: 10.1109/TGRS.2022.3215817.
[32] C. Altuntas and N. Tunalioglu, "Enhancing snow depth estimations through iterative satellite elevation range selection in GNSS-IR to account for terrain variation," *IEEE Trans. Geosci. Remote Sens.*, vol. 61, 2023, Art. no. 5802309, doi: 10.1109/TGRS.2023.3312925.
[33] P. Ma, C. Huang, J. Hou, Y. Zhang, W. Han, and P. Dou, "Snow depth retrieval with multiazimuth and multisatellite data fusion of GNSS-IR considering the influence of surface fluctuation," *IEEE Trans. Geosci. Remote Sens.*, vol. 61, 2023, Art. no. 4302614, doi: 10.1109/TGRS.2023.3323642.
[34] J. Zhan et al., "GNSS-IR snow depth retrieval based on the fusion of multi-satellite SNR data by the BP Neural network," *Remote Sens*, vol. 14, no. 6, Jan. 2022, Art. no. 1395, doi: 10.3390/rs14061395.
[35] C. Altuntas, M. C. Iban, E. Şentürk, U. M. Durdag, and N. Tunalioglu, "Machine learning-based snow depth retrieval using GNSS signal-to-noise ratio data," *GPS Solutions*, vol. 26, no. 4, Aug. 2022, Art. no. 117, doi: 10.1007/s10291-022-01307-2.
[36] W. Liu, X. Yuan, Y. Hu, J. Wickert, and Z. Jiang, "Multifeature GNSS-R snow depth retrieval using GA-BP neural network," *IEEE Geosci. Remote Sens. Lett.*, vol. 20, 2023, Art. no. 2000505, doi: 10.1109/LGRS.2023.3291404.
[37] Y. Hu, X. Yuan, W. Liu, Q. Hu, J. Wickert, and Z. Jiang, "An SVM-based snow detection algorithm for GNSS-R snow depth retrievals," *IEEE J. Sel. Top. Appl. Earth Observ. Remote Sens.*, vol. 15, pp. 6046–6052, 2022, doi: 10.1109/JSTARS.2022.3193113.
[38] Z. Li, P. Chen, N. Zheng, H. Liu, and L. Liu, "Application research and error analysis of GNSS-MR technology in snow depth measurement," in *Proc. China Satell. Navigat. Conf.*, 2020, pp. 129–140.
[39] Q. Wu, K. Wang, H. Zhao, and W. Shi, "Snow depth retrieval using GPS signal-to-noise ratio data based on improved complete ensemble empirical mode decomposition," *GPS Solutions*, vol. 27, no. 4, Sep. 2023, Art. no. 201, doi: 10.1007/s10291-023-01537-y.
[40] K. M. Larson and E. E. Small, "Estimation of snow depth using L1 GPS signal-to-noise ratio data," *IEEE J. Sel. Top. Appl. Earth Observ. Remote Sens.*, vol. 9, no. 10, pp. 4802–4808, Oct. 2016, doi: 10.1109/JSTARS.2015.2508673.
[41] L. S. Haynes et al., "A survey of highly parallel computing," *Computer*, vol. 15, no. 1, pp. 9–24, 1982.
[42] Z. Zhou, K. Yu, J. Bu, Y. Li, and S. Han, "Snow depth estimation based on combination of pseudorange measurements of GNSS geodetic receivers," *Adv. Space Res.*, vol. 69, no. 3, pp. 1439–1450, Feb. 2022, doi: 10.1016/j.asr.2021.11.004.

**Yuan Hu** received the Ph.D. degree in pattern recognition and intelligent system from Shanghai Jiao Tong University, Shanghai, China, in 2011.

She is currently an Associate Professor of Electrical Engineering with Shanghai Ocean University, Shanghai. Her research interests include signal processing, computer science, global navigation satellite system (GNSS)-related application studies, GNSS signal processing, GNSS reflectometry, and the earth deformation studies.

**Jingxin Wang** was born in Anhui, China, in 1999. He received the bachelor's degree in automation from the Anhui University of Science and Technology, Anhui, China, in 2022. He is currently working toward the master's degree in electronic information engineering (control engineering) with the School of Engineering, Shanghai Ocean University, Shanghai, China.

His research interests include application of remote sensing techniques, particularly global navigation satellite system reflectometry, in the context of climate change.

**Wei Liu** received the B.Sc. and M.Sc. degrees in automation and instrument engineering from Northeastern University, Shenyang, China, in 2003 and 2006, respectively, and the Ph.D. degree in guidance, navigation, and control from Shanghai Jiao Tong University, Shanghai, China, in 2011.

From 2015 to 2016, he was with the Department for Geodesy, German Research Centre for Geosciences, Potsdam, Germany. He is currently a Full Professor of Communication and Navigation with Shanghai Maritime University, Shanghai. His research interests include global navigation satellite system (GNSS) signal processing, GNSS reflectometry, and GNSS-related interference studies.

**Xintai Yuan** was born in Guangdong, China, in 1998. He received the bachelor's degree in mechanical engineering from Shantou University, Shantou, China, in 2020, the master's degree in mechanical engineering from Shanghai Ocean University, Shanghai, China, in 2023. He is currently working toward the Ph.D. degree in geodesy and geoinformation science with Technische Universität Berlin, Berlin, Germany.

His research interests include the use of remote sensing techniques, such as global navigation satellite system reflectometry applied to global climate change.

**Jens Wickert** received the bachelor's degree in physics from Technical University Dresden, Dresden, Germany, in 1991, and the Ph.D. degree in geophysics/meteorology from Karl-Franzens-University Graz, Graz, Austria, in 2002.

He was a Principal Investigator of the pioneering GPS radio occultation experiment aboard the German CHAMP. He was also with several German geoscience research institutes. He is currently a joint Professor of Global Navigation Satellite System (GNSS) Remote Sensing, Navigation, and Positioning with the German Research Centre for Geosciences GFZ, Potsdam, Germany, and with the Technical University of Berlin, Berlin, Germany, and also a Chair of the Science Advisory Group of the GEROS-ISS mission for GNSS reflectometry. In addition, he is also the Deputy GFZ Section Head Space Geodetic Techniques and the GFZ Speaker of the Atmosphere and Climate Research Program of the German Helmholtz Association. He has authored or coauthored more than 160 ISI-listed publications on GNSS earth observation.

Dr. Wickert received several research awards.